Supporting Information for:

Speciation Matters: Bioavailability of Silver and Silver Sulfide Nanoparticles to Alfalfa (*Medicago sativa*)

*John P. Stegemeier,[1,2]† Fabienne Schwab,[1,3]† Benjamin P. Colman,[1,4] Sam Webb,[5] Matt Newville,[6] Antonio Lanzirotti,[6] Christopher Winkler,[7] Mark R. Wiesner,[1,3] and Gregory V. Lowry[1,2]**

1 Center for the Environmental Implications of NanoTechnology (CEINT)
2 Civil & Environmental Engineering, Carnegie Mellon University, Pittsburgh, PA 15213, United States
3 Civil & Environmental Engineering, Duke University, Durham, NC 27708, United States
4 Department of Biology, Duke University, Durham, NC 27708, United States
5 Stanford Synchrotron Radiation Lightsource, Stanford University, Menlo Park, CA 94025, United States
6 Advanced Photon Source, Argonne National Lab, Lemont, IL 60439, United States
7 ICTAS Nanoscale Characterization and Fabrication Laboratory, Virginia Tech, Blacksburg, VA 24061, USA

Table of Contents

Figure S1 : Photograph of the alfalfa plants in their holders. Notice the increased mortality and stunted growth in Ag(0)-NPs and $AgNO_3$ compared to other treatments with lower filterable silver concentrations. Hormesis (increased growth) can be observed in the supernatant.

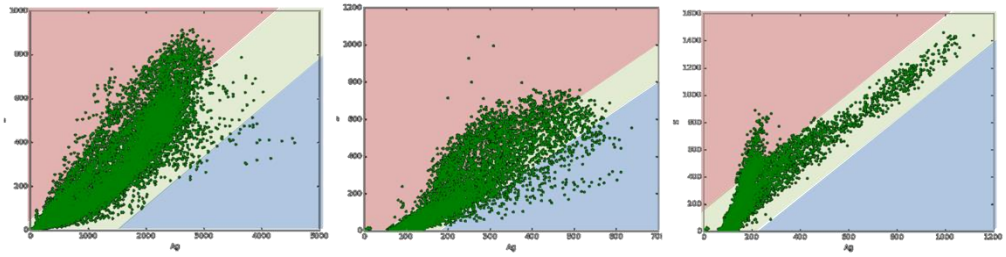

Figure S2: Silver (X axis) vs Sulfur (Y axis) fluorescence count correlation plots for the samples exposed to $AgNO_3$ (left), Ag(0)-NPs (middle) and Ag_2S-NPs (right), with populations identified as high (blue) medium (green) and low (red) Ag:S ratio.

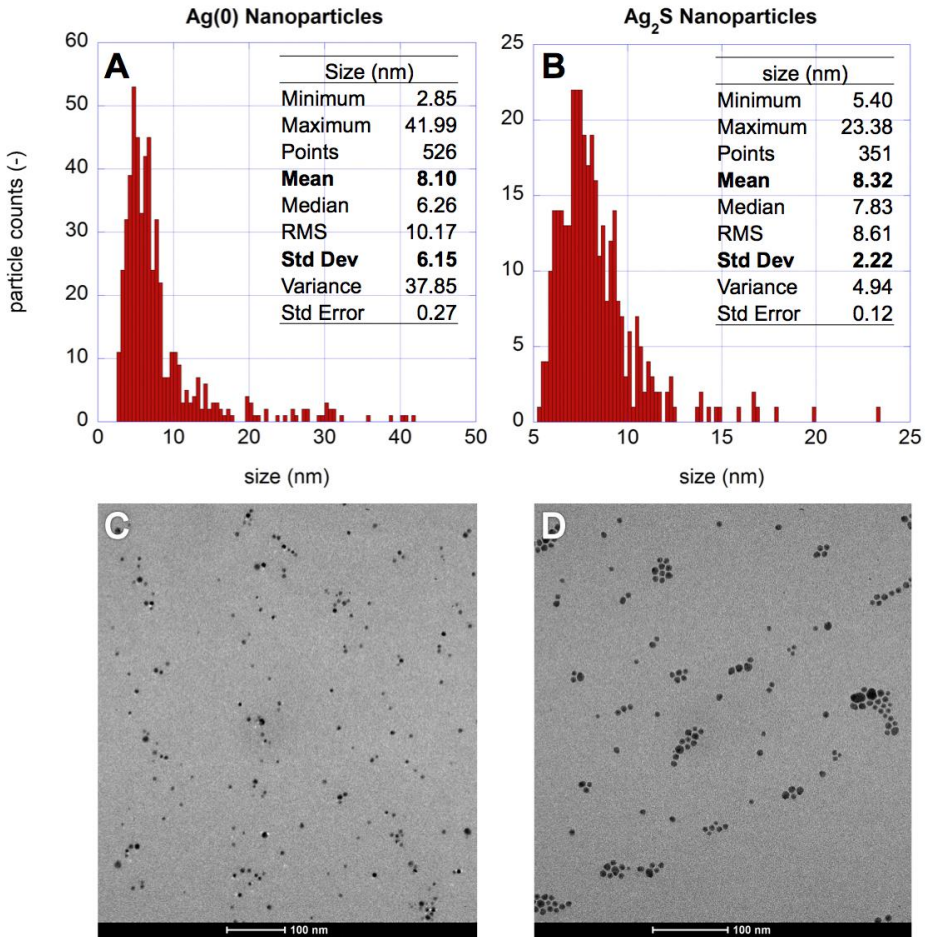

Figure S3: Diameter size distribution of freshly synthesized Ag(0)-NPs, A; and Ag_2S-NPs nanoparticles, B. The diameter of the particles was determined by quantitative image analysis (software: ImageJ 1.0) of transmission electron micrographs as shown in C, Ag(0)-NPs; and D, Ag_2S-NPs. The particles analyzed here were taken from a suspension in half strength Hoagland's medium.

Table S1 (continued next page): Size distribution of the particles in suspension as determined by dynamic light scattering (DLS, continuation next page). The particles were suspended in half strength Hoagland's medium. Only the peaks with maximal intensity are shown.

	Filtered[a]	n^b (-)	Size	±	Stdev	Intensity (%)
100 nm size standard[c]	yes	1	96	±	23	100.0
ultrapure water	yes	1	-	±	-	-
Hoagland's medium[d]	yes	1	(727	±	130)	(100.0)
Ag(0)-NPs	no	3	11.6	±	4.4	92.0
	yes	3	11.6	±	2.9	93.1
Ag_2S-NPs	no	3	(12.8	±	3.7)	(97.9)
	yes	3	16	±	13	100.0

[a]Filtered through a 0.45 µm polytetrafluorethylene (PTFE) filter. [b]Number of replicated measurements. [c]Certified latex standard (Izon, USA) to validate instrument performance. [d]Half strength. [e]Measurements with a polydispersity >0.35 are shown in brackets because highly polydisperse samples, especially if unfiltered, are not accurately measurable using DLS.

Table S1 continuation: Size distribution of the particles in suspension as determined by dynamic light scattering (DLS). The particles were suspended in half strength Hoagland's medium.

	Filtered[a]	n^b (-)	Diffusion Coefficient (μ^2/s)	Count Rate (kcps)	Derived Count Rate[f] (kcps)	PdI (-)
100 nm size standard[c]	yes	1	4.75	415	9,438	0.01
ultrapure water	yes	1	-	-	-	-
Hoagland's medium[d]	yes	1	(0.41)	(167)	(1,506)	(0.52)
Ag(0)-NPs	no	3	4.19	248	68,670	0.28
	yes	3	6.52	405	32,117	0.31
Ag_2S-NPs	no	3	(1.17)	(473)	(473)	(0.42)
	yes	3	7.10	469	469	0.26

[a]Filtered through a 0.45 µm polytetrafluorethylene (PTFE) filter. [b]Number of replicated measurements. [c]Certified latex standard (Izon, USA) to validate instrument performance. [d]Half strength. [e]Measurements with a polydispersity >0.35 are shown in brackets because highly polydisperse samples, especially if unfiltered, are not accurately measurable using DLS. [f]Note that the derived count rate is a function of the particle type and therefore only proportional to particle concentration for particles of the same kind.

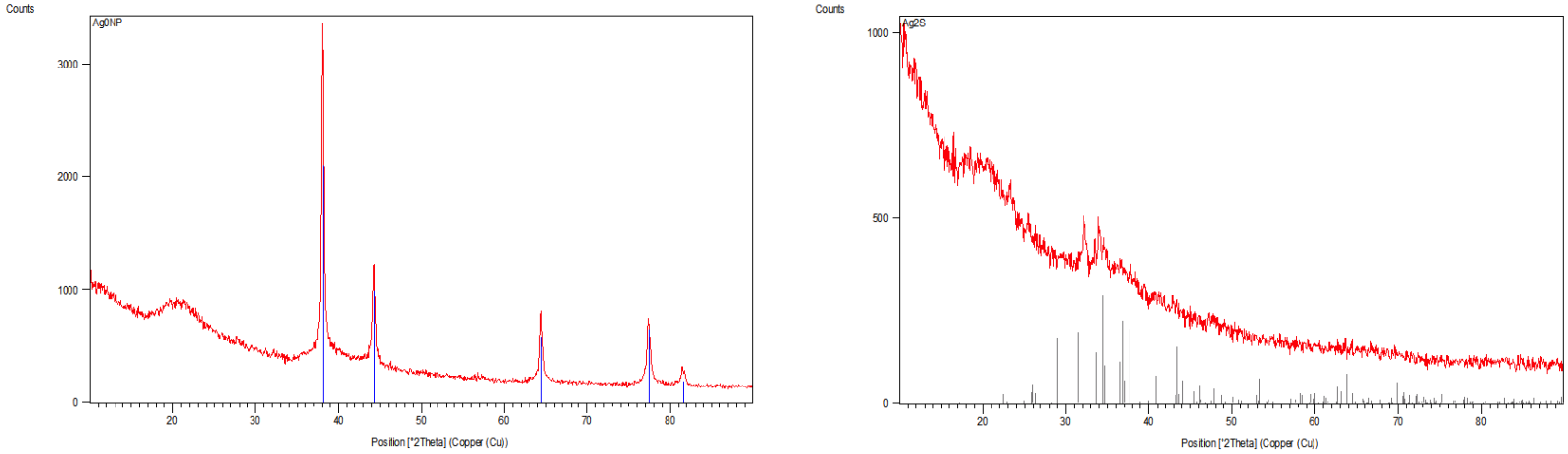

Figure S4 :Ag(0)-NPs (left) and Ag_2S-NPs (right) X-ray powder diffraction spectra after drying at 50 °C with fitted to the reference spectra of metallic silver and acanthite (Ag_2S) .

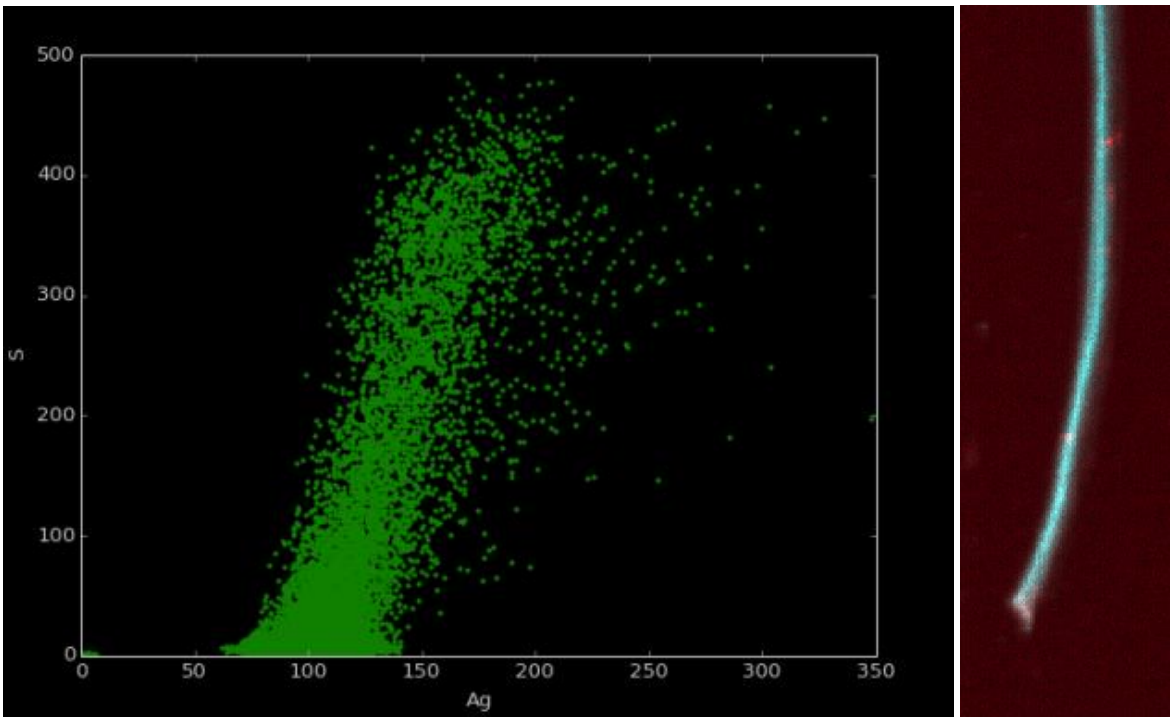

Figure S5: Control alfalfa root tip with Ag/S correlation plot with bi color, which shows potential auto-correlation. The background silver signal, attributed to the fluorescence of argon, is on the order of 100 counts per sec and remains similar for the plant tissue analyzed, suggesting no silver is present in the tissue of control plants.

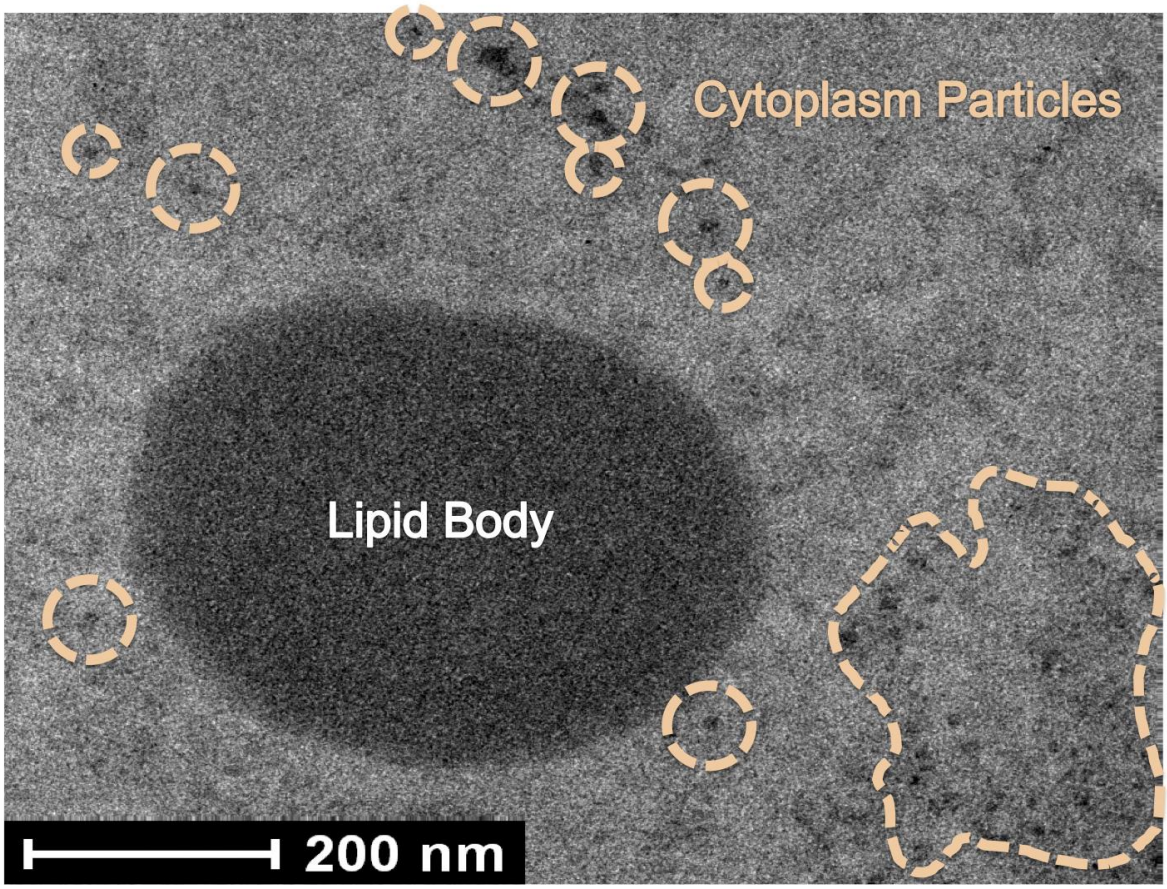

Figure S6: Transmission electron microscopy micrograph showing a magnified lipid body of a control root cell of Alfalfa (*Medicago sativa*). The spherical electron dense (i.e. dark) region outlines the structure of the lipid body. Note the highly electron dense particles in the cytoplasm (highlighted by peach broken lines, likely Si as observed by energy dispersive X-ray spectroscopy in comparable regions of the cytoplasm).

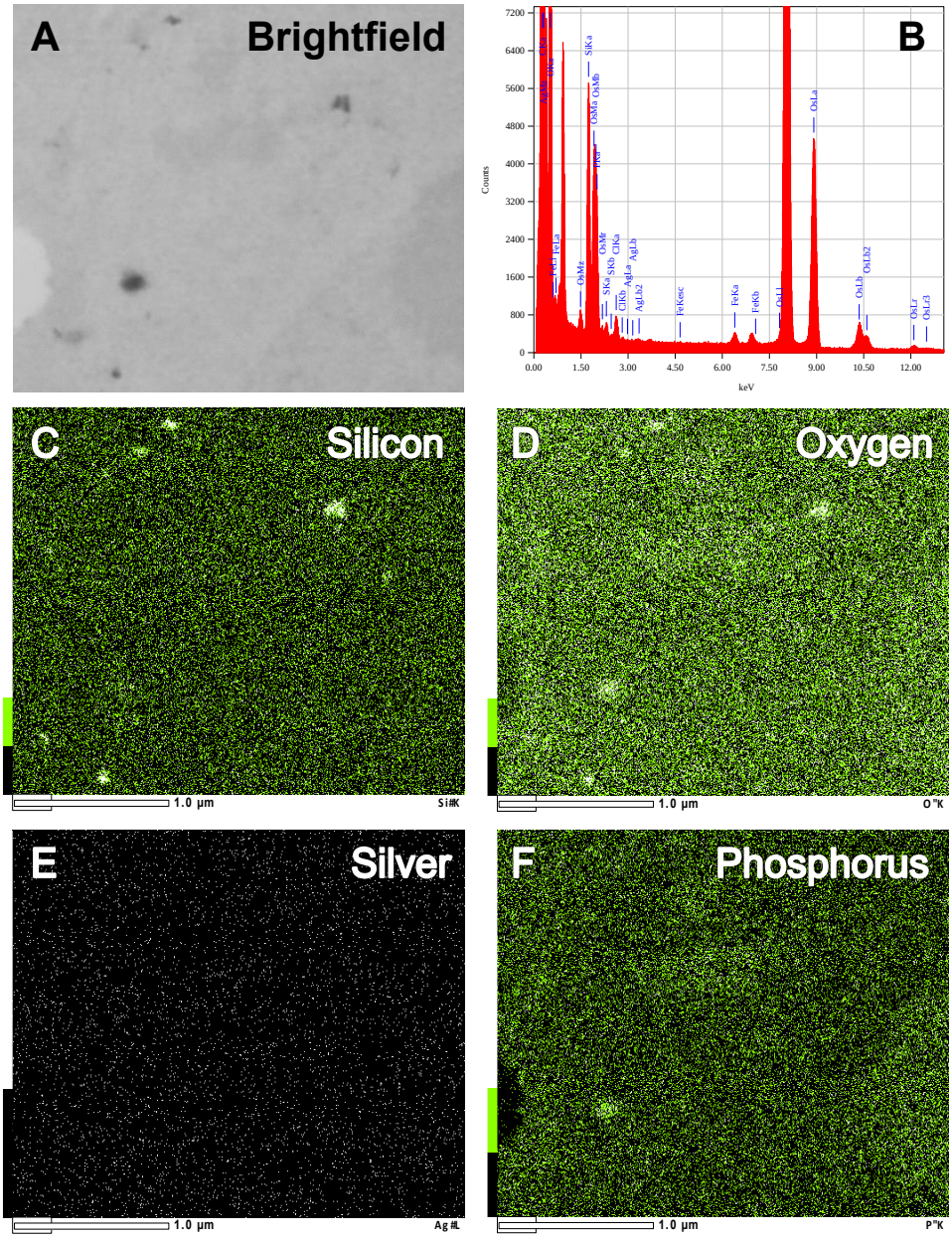

Figure S7: Transmission electron microscopy (TEM) coupled with energy dispersive X-ray spectroscopy (EDS) of particles in the cytoplasm of alfalfa exposed to Ag_2S-NPs nanoparticles. The cytoplasmic region shown is comparable to P at a higher magnification. A: Phase contrast image of similar aggregates in the cytoplasm as visible in P. The aggregates can be seen in the phase contrast image as dark spots. The line scan shows elevated signals of Si and O. B: The energy spectrum of the same region as in A shows a strong Si peak. C: Mapping shows that Si is concentrated on all but one aggregate in the cytoplasm, whereas no aggregates of Ag are visible. D: Oxygen is concentrated, too, on the nano-sized aggregates, confirming the presence of Si in the form of nano-Si_yO_X. The ratio of Si:O counts was ~1:2.

Table S2: Diameters of electron dense particles and aggregates measured by transmission electron microscopy in different cell compartments of the root tip. Underlined values were significantly different from the same particle type in the control (One-way analysis with unequal variances, Levene statistics $p<0.001$, Dunnett's C post-hoc analysis at a 95% significance level). Italicized values are particles that were exclusively present in exposed plant cells.

Treatment	Particle Morphology	*N*	Diameter (nm)				
			Average	Median	Stdev	Min	Max
Control	Cytoplasm Particles	52	7.9	7.1	3.1	2.9	15.3
	Vacuole Aggregates	45	61	39	53	10	243
AgNO3	Cytoplasm Particles	66	7.9	8.0	3.9	1.5	17.9
	Cytoplasm Aggregates	49	*33*	29	18	12	90
	Cytoplasm + Vacuole Round Particles	41	*102*	77	61	32	278
Ag(0)-NPs	Border Cell Adsorbed Particles	62	*74*	72	17	33	133
	Cell Wall Particles	46	*2.52*	2.43	0.83	1.25	4.78
	Cytoplasm Particles	63	9.9	9.2	4.9	1.0	30.1
	Cytoplasm Aggregates	8	*55*	51	17	32	86
	Vacuole Aggregates	26	74	54	48	22	209
Ag_2S-NPs	Border Cell Adsorbed Particles	68	84	76	34	32	205
	Cell Wall Particles	81	*2.54*	2.55	0.77	0.93	4.94
	Cytoplasm Particles	38	<u>17.2</u>	14.7	7.8	6.6	36.9
	Cytoplasm Aggregates	17	*96*	112	35	49	164
	Vacuole Aggregates	44	<u>230</u>	187	189	17	794

Table S3: Maximum x-ray count attributed to Ag for K-edge XRF map (Figure 2) and attributed to Ag and S the L-edge Ag XRF map (Figure 3).

	Fig 2 Ag Counts	Fig 3 Ag counts	Fig 3 S counts
Ag(0)-NPs	1837	637	1042
Ag_2S-NPs	3406	1117	1459
$AgNO_3$	N/A	4571	914

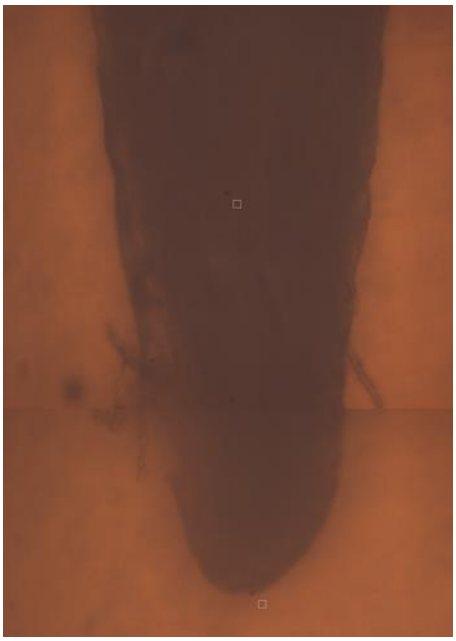

Figure S8: Light micrograph image of root tip used to generate the outline in Figure 2.

Miscellaneous other electron dense particles observed by TEM

The large, round, highly electron dense particles in the vacuoles of the $AgNO_3$-exposed root cells were most probably similar re-precipitated Ag(0) particles as reported in previous studies.[48] Due to the high electron density of these particles the contrast of the rest of these cells was very low (Figure 4 F, I). The central vacuoles of most cells in all treatments contained electron dense aggregates (Figure 4A, I, N, and S, Figure 5 & Table S2), which are known to be various detoxification products of the cell. The >100 nm sized, round, moderately electron dense objects in Figure 4 A, E, J, P, and S were identified as lipid bodies under higher magnification (example in Figure S6). The vacuole containing four smaller vacuoles in Figure 4 P is most probably a peroxysome. The crescent-shaped shadows on the starch grains in Figure 4 J did mainly contain elevated concentrations of Os which evaporated when the samples rested under the beam for >1 min. It is unclear why these shadows only formed in the $AgNO_3$-exposed roots. Probably these cells produced increased amounts of lipids near the starch grains, however, the lipid content of these cells was not analyzed.